

The First High-Resolution Spectra of 1.3 L Subdwarfs

A. Reiners^{1,*}

and

G. Basri

Astronomy Department, University of California, Berkeley, CA 94720

[areiners, basri]@astron.berkeley.edu

ABSTRACT

We present the first high-resolution ($R \approx 31\,000$) spectra of the cool sdL 2MASS 0532+8246, and what was originally identified as an early-type L subdwarf (sdL) LSR 1610–0040. Our work, in combination with contemporaneous work by Cushing and Vacca, makes it clear that the latter object is more probably a mid-M dwarf with an unusual composition that gives it some sub-dwarf spectral features. We use the data to derive precise radial velocities for both objects and to estimate space motion; both are consistent with halo kinematics. We measure the projected rotational velocities, revealing very slow rotation for the old sd?M6 object LSR 1610–0040. 2MASS 0532+8246 exhibits rapid rotation of $v \sin i = 65 \pm 15 \text{ km s}^{-1}$, consistent with the behavior of L dwarfs. This means that the braking time for L dwarfs is extremely long, or that perhaps they never slow down.

A detailed comparison of the atomic Rb and Cs lines to spectra of field L dwarfs shows the spectral type 2MASS 0532+8246 is consistent with being mid-to late-L. The Rb I and K I lines of LSR 1610–0040 are like an early-L dwarf, but the Cs I line is like a mid-M dwarf. The appearance of the Ca II triplet in absorption in this object is very hard to understand if it is not as least as warm as M6. We explain these effects in a consistent way using a mildly metal-poor mid-M model. M subdwarfs have weak metal-oxides and enhanced metal-hydrides relative to normal M dwarfs. LSR 1610–0040 exhibits metal-hydrides like an M dwarf but metal-oxides like a subdwarf. The same explanation that resolves the atomic line discrepancy explains this as well.

¹Hamburger Sternwarte, Universität Hamburg, Gojenbergsweg 112, D-21029 Hamburg, Germany

* Marie Curie Outgoing International Fellow

Our spectra cover the spectral region around a previously unidentified absorption feature at 9600 Å, and the region around 9400 Å where detection of TiH has been claimed. We identify the absorption around 9600 Å as due to atomic lines of Ti and a small contribution of FeH, but we cannot confirm a detection of TiH in the spectra of cool L subdwarfs. In 2MASS 0532+8246, both metal-oxides *and* metal-hydrides are extremely strong relative to normal L dwarfs. It may be possible to explain the strong oxide features in 2MASS 0532+8246 by invoking effects due to inhibited dust formation. High resolution spectroscopy has aided in beginning to understand the complex molecular chemistry and spectral formation in metal-deficient and ultracool atmospheres, and the properties of early ultralow-mass objects.

Subject headings: stars: low mass, brown dwarfs - stars: chemically peculiar - subdwarfs - stars: individual(LSR J1610-0040, 2MASS J05325346+8246465)

1. Introduction

The most immediate relics of the early Galaxy are the cool subdwarfs of spectral type sdK and later – lifetimes of such cool stars are well in excess of the age of the Galaxy. Their metal-deficient atmospheres make them appear hotter than solar-metallicity main-sequence stars of the same mass, which in turn renders them “subluminous” (Kuiper 1939).

The spectral classification of solar abundance K- and M-dwarfs is well understood, and is entirely due to changes in effective temperature. Classification of M-subdwarfs is based on the metallicity sensitive ratio of absorption bands of metal-oxides and metal-hydrides (Gizis 1997; Lépine et al. 2003a); metal-hydrides are generally stronger in metal-deficient atmospheres, while metal-oxides are weaker (e.g., Mould 1976). In the ultracool atmospheres of late M- and L-dwarfs, however, refractory grains become an important ingredient since they are competing with molecules for available metals. Furthermore, their opacity influences the optical depth, and hence which part of the atmosphere is visible. Since the formation and distribution of dust grains is not well understood even in solar abundance stars, this is an even more severe problem in the classification of metal-deficient L-subdwarfs.

The last two years have seen the first discoveries of L-type subdwarfs. These ultracool dwarfs exhibit colors too red for an M-type object, and do not fit on the expanded subdwarf classification scheme of Lépine et al. (2003a). Another argument for surface temperatures lower than M-dwarf temperatures is the extremely strong absorption lines of alkali atoms as K I, Na I, and Rb I. The first L-type subdwarf, 2MASS J05325346+8246465 (hereafter

2MASS 0532+8246), was discovered by Burgasser et al. (2003, hereafter B03). Its spectrum is very similar to the L7 dwarf DENIS 0205–1159 AB, exhibiting strong alkali lines (we use the optical classification scheme of Kirkpatrick et al. 1999). 2MASS 0532+8246 shows enhanced metal hydride bands, but in contrast to M-subdwarfs it also has strongly enhanced bands of TiO. The first proposed early-type L-subdwarf, LSR 1610–0040, was discovered by Lépine et al. (2003b, hereafter L03). It also exhibits strong Rb I absorption and L03 report enhanced CaH and TiO bands. Metal hydrides FeH and CrH, however, are relatively weak. We conclude in this paper that LSR 1610–0040 is not really an L subdwarf, but in the M temperature range. The same conclusion is reached in a paper based on lower resolution spectra that was posted during our refereeing process by Cushing & Vacca (2005, hereafter CV05). The spectral peculiarities of these unusual objects provide a preview of the complex chemical processes occurring in cool atmospheres of metal-deficient L-dwarfs. The list of subdwarfs of spectral type L and late M is constantly growing; Burgasser (2004a) discovered the L-subdwarf LSR 1626 + 3925, and two late M-type subdwarfs at the end of the subdwarf classification scheme with features very similar to the L-type subdwarfs have been reported by Scholz et al. (2004a, SSSPM J1013–1356) and Scholz et al. (2004b, SSSPM J1444–2019).

The presumably large age of M- and L-subdwarfs also makes them ideal tracers of the rotational evolution of late-type objects. Cool stars of spectral type K and M are known to suffer rotational braking on a relatively short timescale (1 Gyr), but no projected rotation velocity below $v \sin i = 10 \text{ km s}^{-1}$ has been reported in an L-dwarf (Mohanty & Basri 2003; Bailer-Jones 2004). Whether this is due to extremely long braking times or the lack of rotational braking at all in L-dwarfs may be answered by observations of the rotation of the oldest objects of very late spectral type.

So far, no high-resolution spectrum of an L-type subdwarf has been available to investigate the details of line strengths, take a close look for unidentified features detected in L-subdwarf spectra, (among them the tentative detection of TiH, Burgasser et al. 2004b), and to investigate rotation velocities. In this paper, we present the first high resolution spectra of the late-type sdL 2MASS 0532+8246 and the peculiar sd?M LSR 1610–0040. We describe our observations in § 2. Radial velocities are calculated in § 3, where we also derive new constraints on the space motion on the basis of the accurate radial velocities. Surface rotation is investigated in § 4, and individual spectral features are discussed in § 5.

2. Observations

Both targets were observed with HIRES at Keck I on March 2, 2005, after the detector upgrade. The spectral sensitivity and coverage are substantially improved after the upgrade,

allowing us to obtain high-resolution spectra of these faint objects, especially in the CCD infrared. With the new CCD mosaic we were able to cover the spectral region from 5700 Å to 1 μm in 25 spectral orders. In the red part of the spectrum, however, spectral coverage is still incomplete. The CCD mosaic is made of three chips; two spectral orders fall onto the gaps and could not be observed.

We obtained a signal-to-noise ratio (SNR) better than 30 around 8000 Å in a 40 min exposure of LSR 1610–0040. The much fainter 2MASS 0532+8246 was observed for 45 min yielding much lower a SNR in the optical wavelength region. However, due to the improved sensitivity in the red CCD, we achieved a SNR well above ten in the near infrared region redward of 8500 Å.

We positioned the CCD mosaic in order to obtain the spectral features most important in late-type stars and brown dwarfs. Our spectra include the important alkali lines of Rb I and Cs I, the TiO band at 8450 Å the prominent FeH and CrH bands at 1 μm , the TiH region at 9400 Å, and the unidentified spectral feature around 9600 Å (B03). On the other hand, we were not able to cover the Na I resonance doublet in the same exposure, and we miss the FeH and CrH bands at 8600 Å and 8700 Å since they fall in the gap between two of the CCDs. The TiO band at 7040 Å and the K resonance lines are at the very edge of our spectra.

3. Radial velocities and space motion

We calculate the radial velocities of LSR 1610–0040 and 2MASS 0532+8246 by comparison to the radial velocity of Gl 406 ($v_{\text{rad}} = 19 \pm 1 \text{ km s}^{-1}$, Martín et al. 1997), which was observed during the same night. Radial velocities are measured from a cross correlation with the spectrum of Gl 406 and applying the barycentric corrections. We give all parameters of LSR 1610–0040 and 2MASS 0532+8246 in Tables 1 and 2, respectively.

3.1. 2MASS 0532+8246

To calculate the radial velocity of 2MASS 0532+8246, we employ two spectral orders covering the regions around 9200 Å and before 1 μm where strong features of FeH are dominant. After barycentric correction, we calculate a relative radial velocity between 2MASS 0532+8246 and Gl 406 of $\Delta v_{\text{rad}} = -191 \pm 1 \text{ km s}^{-1}$, i.e., $v_{\text{rad}} = -172 \pm 1 \text{ km s}^{-1}$. This result is within 2σ of the value reported by B03 ($v_{\text{rad}} = -195 \pm 11 \text{ km s}^{-1}$). In fact, B03 observe a stronger blueshift when they derive v_{rad} from optical Cs I and Rb I lines. The radial

Table 1. Parameters of LSR 1610–0040

Parameter	Value
R.A. (J2000.0)	$16^h10^m28^s.85$
Decl. (J2000.0)	$-00^\circ40'53''.0$
μ^a	$1''.46 \text{ yr}^{-1}$
θ^a	$212^\circ0$
Distance ^a	$16 \pm 4 \text{ pc}$
2 MASS J	$12.91 \pm 0.02 \text{ mag}$
2 MASS H	$12.32 \pm 0.02 \text{ mag}$
2 MASS K_s	$12.02 \pm 0.03 \text{ mag}$
v_{rad}	$-95 \pm 1 \text{ km s}^{-1}$
U	$-44 \pm 8 \text{ km s}^{-1}$
V	$-111 \pm 27 \text{ km s}^{-1}$
W	$-51 \pm 2 \text{ km s}^{-1}$
$v \sin i$	$< 5 \text{ km s}^{-1}$

^aLépine et al. (2003b)

Table 2. Parameters of 2MASS 0532+8246

Parameter	Value
R.A. ^a	$5^h 32^m 53^s.46$
Decl. ^a	$+82^\circ 46' 46''.5$
μ^b	$2''.60 \pm 0''.015 \text{ yr}^{-1}$
θ^b	$130^\circ.0 \pm 1^\circ.8$
Distance ^c	$20 \pm 10 \text{ pc}$
2 MASS J	$15.81 \pm 0.06 \text{ mag}$
2 MASS H	$14.90 \pm 0.10 \text{ mag}$
2 MASS K_s	$14.92 \pm 0.15 \text{ mag}$
v_{rad}	$-172 \pm 1 \text{ km s}^{-1}$
$v \sin i$	$65 \pm 15 \text{ km s}^{-1}$

^aEpoch 1999 March 1 (UT),
Burgasser et al. (2003)

^bBurgasser et al. (2003)

^cestimate from optical spectrum,
Burgasser et al. (2003)

velocity they derive from infrared K I lines at $1.1690/1.1773\ \mu\text{m}$, $\langle v_{\text{rad}} \rangle = -175 \pm 17\ \text{km s}^{-1}$, matches much better with our value from high resolution spectra.

In order to estimate the space motion of 2MASS 0532+8246, we adopt the parameters given by B03. Assuming that the spectroscopically derived I_C -magnitude of 2MASS 0532+8246 is similar to late-type L dwarfs, they estimate a distance of $d = 10 - 30\ \text{pc}$. The radial velocity we derive from our data only yields small corrections to the space motion vector they give, the new result is $[U, V, W] = [-26, -285, 38]\ \text{km s}^{-1}$. However, due to the uncertain distance, the space motion is poorly constrained and we do not include it in Table 2. Nevertheless, the likelihood of a very high V -velocity 2MASS 0532+8246 does significantly exceed the 2σ limit for disk stars, as was mentioned by B03.

3.2. LSR 1610–0040

For LSR 1610–0040, we use three spectral orders around $8000\ \text{\AA}$. We checked the reliability of our radial velocity determination by measuring v_{rad} for GJ 299, GJ 1227 and GJ 1111 from observations taken during the same night. In all three cases our results show excellent agreement with the values reported in Delfosse et al. (1998) and Mohanty & Basri (2003). The relative velocity difference between LSR 1610–0040 and Gl 406 as calculated from the spectra is $\Delta v_{\text{rad}} = -113.7 \pm 0.2\ \text{km s}^{-1}$ after barycentric correction. Our uncertainty is dominated by the star’s position in the slit, and we estimate a systematic uncertainty of $1\ \text{km s}^{-1}$. Thus, for LSR 1610–0040 we calculate a radial velocity of $v_{\text{rad}} = -95 \pm 1\ \text{km s}^{-1}$.

This results is not in agreement with the radial velocity of $v_{\text{rad}} = -130 \pm 15\ \text{km s}^{-1}$ reported by L03. However, B03 calculated v_{rad} for 2MASS 0532+8246 and found a difference between their values of v_{rad} derived from optical and from infrared wavelength regions (see Sect. 3.1). Using low resolution data at optical wavelengths they obtain a radial velocity that is about $20\ \text{km s}^{-1}$ more blueshifted than v_{rad} derived from infrared regions. As was mentioned above, our results agree with the result they get from the infrared data. We suggest that such an offset is also the reason for the mismatch between the radial velocity derived in low-resolution data at optical wavelengths by L03 and the value we derive from our high-resolution data. If we correct the radial velocity reported by L03 by the $+20\ \text{km s}^{-1}$ reported by B03, the corrected value is $v_{\text{rad}} = -110 \pm 15\ \text{km s}^{-1}$, which is consistent with the value of $v_{\text{rad}} = -95 \pm 1\ \text{km s}^{-1}$ we find.

To calculate the space motion vector $[U, V, W]$, we first tried to reproduce the vector

reported by L03. We use the IDL procedure `gal_uvw`¹ and the coordinates, proper motion and radial velocity given in L03. However, we do not derive the same space motion (while we do get the identical vector B03 derive for 2MASS 0532+8246). Our result is $[-72, -117, -71] \text{ km s}^{-1}$, while L03 report $[-111, -85, -24] \text{ km s}^{-1}$ (they also write slightly different values in their Table 1 and their Sect. 5). Including the new radial velocity for LSR 1610–0040 we derive our final result of $[U, V, W] = [-44, -111, -51] \text{ km s}^{-1}$. This places LSR 1610–0040 inside the 2σ limit of thick disk stars, as defined by Chiba & Beers (2000). Nevertheless, the V -velocity of LSR 1610–0040 of $-111 \pm 27 \text{ km s}^{-1}$ still is indicative of halo kinematics, although it is not statistically significant in comparison to the sample of Chiba & Beers (2000).

4. Rotation velocities

The predominant spectral features visible in L-type spectra are molecular bandheads and strongly pressure-broadened alkali lines. Neither of them allow a determination of $v \sin i$ by directly fitting a rotationally broadened template to the spectrum, as can be successfully done in hotter stars where the shape of unblended atomic lines indicate stellar rotation very precisely. The projected rotation velocities $v \sin i$ of ultralow mass objects as late as spectral type L are usually determined via cross-correlation with a slowly rotating M- or L-type object used as a template (Basri et al. 2000). The spectral type of the template star should be as close as possible to the target. One of the latest slow rotating M-dwarfs bright enough to be employed as a template star is Gl 406 (M5.5), and that star is often used for the cross-correlation technique also in L-dwarfs. It is not entirely clear to what extent spectral differences between the spectra of M- and L-type dwarfs, e.g. the severe broadening of alkali lines in L-dwarfs, could mimic a higher rotation velocity when using an M-dwarf template to derive $v \sin i$ in an L-dwarf. Mohanty & Basri (2003) discuss this issue in detail. Bailer-Jones (2004) used the spectrum of 2MASS 1439+1929 (L1.0, $v \sin i \approx 10 \text{ km s}^{-1}$) to calculate $v \sin i$ in his L-dwarf sample. He found no significant differences between the two values of $v \sin i$ he individually derived from a cross-correlation with Gl 406, and with 2MASS 1439+1929. This supports the assumption that using an M-dwarf for the template does in fact yield the correct $v \sin i$ as well.

The slowest projected rotation velocity measured in an L-dwarf is as high as $v \sin i \approx 10 \text{ km s}^{-1}$ (Mohanty & Basri 2003; Bailer-Jones 2004), while mid-M dwarfs are mixed and early-M dwarfs usually have rotation velocities below the detection limit. L-dwarfs may not

¹<http://idlastro.gsfc.nasa.gov/contents.html>

suffer rotational braking at all, since their neutral atmospheres could inhibit any kind of magnetic coupling that is the source of rotational braking in hotter stars (Mohanty et al. 2002). However, flares have been observed to occur in L-dwarfs and some are observed to exhibit $H\alpha$ emission (Leibert et al. 2003). This indicates at least the possibility of magnetic braking. The lack of slowly rotating L-dwarfs could also be an artifact of observing predominantly young objects since they are simply brighter than older objects of the same mass. In that case slow rotators might be found among the very oldest L-dwarfs, the subdwarf population.

We calculated the cross-correlation functions of our target stars LSR 1610–0040 and 2MASS 0532+8246 with Gl 406 in several spectral orders. Results from different spectral orders are consistent with each other. The cross-correlation functions of LSR 1610–0040 and 2MASS 0532+8246 from the wavelength region around 9150 Å are shown in the left and right panels of Fig. 1, respectively. To calibrate the width of the cross-correlation functions, we spun up the spectrum of Gl 406 according to surface velocities $v \sin i = 20, 40, 60$ and 80 km s^{-1} and calculated the cross-correlation functions with the unbroadened template of Gl 406. The results are overplotted in both panels of Fig. 1 as dashed lines.

It is immediately clear from the left panel of Fig. 1 that LSR 1610–0040 does not show any signs of a rotation faster than Gl 406 ($v \sin i \approx 3 \text{ km s}^{-1}$). This can be viewed as support for the proposition that LSR 1610–0040 is more similar to Gl 406 than an early L dwarf (which is expected to be a rapid rotator).

One advantage of the cross-correlation technique is its applicability to spectra of relatively low signal. The SNR of our spectrum of 2MASS 0532+8246 is much lower because of the faintness of object. Nevertheless, it is possible to derive reliable cross-correlation functions and determine the projected rotation velocity as shown in the right panel of Fig. 1. From that function, we derive a value of $v \sin i = 65 \text{ km s}^{-1}$ for 2MASS 0532+8246. The uncertainty of our result can be derived from comparing results from different spectral orders; we estimate an uncertainty of 15 km s^{-1} (rapid rotation is more difficult to be precise with). If 2MASS 0532+8246 is a relic of the early Galaxy, we are led to the conclusion that the braking time is longer than the age of the Galaxy or there is no braking at all for such cool objects.

5. Spectra of Individual Objects

5.1. LSR 1610–0040

LSR 1610–0040 was proposed as an early-type L-subdwarf by L03. They find its spectral energy distribution to be completely inconsistent with a spectral type sdM6.0, which would be the spectral classification on the basis of the standard classification scheme developed by Gizis (1997) and expanded by Lépine et al. (2003a). On the other hand, CV05 find a good overall fit with a normal M6 dwarf. A second strong argument for a spectral type early L are the Rb I lines, which are atypically strong for a normal M dwarf. We show several spectral orders of our high resolution spectrum of LSR 1610–0040 in Figs. 2 and 3. As a comparison, we overplot the spectra of the M-dwarf Gl 406 (M5.5) and the early-type L-dwarf 2MASS 1439+1929 (L1.0) that we obtained during the same night. The most interesting spectral features in ultra low-mass objects and metal-poor subdwarfs are the metal-oxides, the metal-hydrides, and the strongly pressure-broadened atomic lines of alkali and alkali earth elements. In the following, we discuss the relevant features that are visible in our spectra.

5.1.1. *Metal oxides*

The metal oxides TiO and VO are the main opacity sources in late M-stars. Our spectrum covers three bandheads of TiO, the γ -system at 7050 Å, the ϵ -system at 8430 Å, and the infrared δ -system at 8870 Å. TiO bands are observed to become stronger with cooler effective temperature among early to mid-type M-stars. In the field dwarfs, the TiO bands in late M-dwarfs show a reversal, the γ -band reaches a maximum near M6.5, the ϵ -band has its maximum a little later at M7.5 (Mohanty et al. 2004). The weakening of TiO band-strengths in very late M-dwarfs and early L-dwarfs can be explained by the formation of more metal-rich condensate minerals (Lodders 2002, eg.), i.e. by the formation of dust in metal-rich field dwarfs. Furthermore, dust opacity increases with shorter wavelength and the effects of dust should be visible at bluer wavelengths first.

The reddest TiO band at 8900 Å is displayed in the first panel of Fig. 3. The absorption in LSR 1610–0040 is consistent with the one in Gl 406 and maybe a little weaker than in 2MASS 1439+1929, although this band does not show a clear structure and differences between the three spectra are small. The ϵ -bands at 8450 Å appear very similar in the field M- and L-dwarfs since they lie on both sides of the reversal. The ϵ -band of LSR 1610–0040 is much weaker, indicating metal deficiency or a temperature outside the M5.5–L1 region. The third TiO band at 7050 Å, the γ -band shown in the upper right panel of Fig. 2, is very

strong in LSR 1610–0040. It is consistent with the strong absorption observed in Gl 406 and much weaker than in 2MASS 1439+1929. The weakness of this band in the L1-dwarf is likely due to the onset of dust formation. The band is severely saturated in the two other spectra. At such strong saturation, the underlying opacity could be different in LSR 1610–0040 and Gl 406 while producing the same appearance in the γ -band. Thus, the TiO bands are not inconsistent with the hypothesis, that LSR 1610–0040 is a metal-deficient M-dwarf.

Our spectrum also includes the VO band at 7900 Å, and we confirm the finding by L03 that VO is not strong in LSR 1610–0040. In Gl 406 this band is comparably weak, and even in 2MASS 1439+1929 VO is not particularly strong. This means that no clear conclusions about the temperature or metallicity of LSR 1610–0040 can be drawn from the VO bands. CV05 discuss a possible new set of bands of TiO (and perhaps H₂O) at 9200–9400 Å (their Fig. 6), but suggest that higher resolution spectra are needed for confirmation. We see no evidence for TiO in this region, only a lot of telluric lines.

5.1.2. *Metal hydrides*

In metal poor M-dwarfs, metal hydrides are observed to be much stronger than metal oxides, which is likely due to the competition with H₂O for oxygen (Mould 1976). In LSR 1610–0040, the hydride bands are comparable to those in Gl 406. For example, the CaH band at 6800 Å is comparable to the one in Gl 406 (upper left panel in Fig. 2). The FeH band at 9900 Å is also of comparable strength in the last panel of Fig. 3. These results imply that LSR 1610–0040 is not very metal-poor compared to Gl 406.

In 2MASS 1439+1929 (L1), one expects the FeH band at 9900 Å to be stronger because the star is cooler, and this is seen in last panel of Fig. 3. On the other hand, the upper left panel of Fig. 2 shows that the individual CaH features are weaker in 2MASS 1439+1929 than in the other two objects as is typically observed (although the reason for this is not really known). We note that the normalization in this panel is local; the right upper panel shows that if the spectrum is normalized at 7050 Å, then the L1 spectrum lies above the other two. This likely indicates that the background opacity (TiO?, VO?) is weaker in the L dwarf than in LSR 1610–0040, probably due to dust formation in the former.

Andersson et al. (2003) suggest that absorption features of TiH could become visible in spectra of ultralow mass stars, and Burgasser et al. (2004b) claim a first detection of TiH around 9400 Å in 2MASS 0532+8246 (see Sect. 5.2). We compare the spectra of LSR 1610–0040 and 2MASS 1439+1929 in the second panel of Fig. 3. In this spectral order, we did not adjust the two spectra for their radial velocities in order to match the telluric H₂O features

that are visible in that wavelength region. We included a telluric reference spectrum from HR 153 (spectral type B2) demonstrating that in LSR 1610–0040 all significant absorption features in that wavelength region are due to telluric features. Individual TiH lines from the $^4\Phi - X^4\Phi$ band are indicated (Andersson et al. 2003). No extra absorption due to TiH is visible in the spectrum of LSR 1610–0040 (9380–9407 Å).

5.1.3. Atomic lines

The only strong atomic lines commonly found in spectra of ultralow mass stars are lines of neutral alkali elements, as Na I, K I, Rb I and Cs I, and some alkali earth elements. Such atoms are not captured in refractory grains and remain in the cool atmospheres of L-dwarfs. By far the strongest lines are the ones due to the Na I and K I resonance doublets. Our observations unfortunately do not cover the Na I doublet at 8190 Å, but CV05 show they are strong. Our spectra do cover one of the K I resonance lines at 7700 Å, and this K I line in LSR 1610–0040 is shown in comparison to Gl 406 (M5.5) and 2MASS 1439+1929 (L1.0) in the second panel of Fig. 2. The K I line of LSR 1610–0040 falls between the two comparison spectra; it is significantly stronger than in Gl 406 and it is also stronger than in any field M-dwarf spectrum we have observed.

The suggestion of an early L-type spectral class of LSR 1610–0040 comes in part from the Rb I lines. According to L03, their strengths are the main difference between the spectrum of LSR 1610–0040 and that of the sdM8.0 star LSR 1425 + 7102. Two strong lines of Rb I are covered by our observations, and they are plotted in the second and third panels of Fig. 2. Both lines are observed at high SNR and accurately resemble the shape of the Rb I lines in 2MASS 1439+1929, while they are much stronger than in Gl 406. During our observing run we also observed two dwarfs of spectral type M9, LHS 2065 and LHS 2924. Both show Rb I lines significantly weaker than those observed in LSR 1610–0040 and 2MASS 1439+1929. Thus, the behavior of the atomic lines of K I and Rb I in our high-resolution spectrum confirms that these lines appear typical of a field early-L dwarf.

The observed line strengths of the alkali elements K I and Rb I (and the strong lines of Na I visible in low resolution spectra of CV05) lead us to expect strong lines of Cs I as well. Several Cs I lines are covered by our spectrum; the two lines at 8520 Å and 8944 Å are shown in the last panel of Fig. 2 and the first panel of Fig. 3, respectively. Both lines are remarkably weaker than in 2MASS 1439+1929; the one at 8520 Å is about half as strong as in 2MASS 1439+1929, while the one at 8944 Å is hardly detected at all. This behavior is not consistent with an early-L object.

On the other hand, the Cs I line is stronger than in Gl 406, though not as comparatively strong as the Rb I lines. Both Cs I lines are located directly inside TiO-bands, which are weakened at lower metallicity. The reduced TiO opacity should enhance the visibility of atomic lines. That explanation is supported by the presence of a relatively strong line from Ba I at 8560 Å (another line of Ba I is detected at 7912 Å inside a VO band). Most interesting is the clear detection of two of the Ca II triplet lines (at 8498 and 8542 Å). All these lines with strengths greater than in Gl 406 (which doesn’t really show them at all). The triplet lines require photospheric conditions hot enough to produce ionized calcium, and tend to disappear at M6 except in very active stars (Gl 406 itself is reasonably active, and yet does not show them). Taken together, these results are consistent with a mid-M effective temperature, but with weakened background opacity due to a lower metallicity.

Our spectrum also covers the wavelength region around 9600 Å, where B03 and Bur-gasser (2004a) report the detection of a so far unidentified absorption feature. We show that region in the third panel of Fig. 3. In the spectrum of LSR 1610–0040, six individual absorption features appear between 9580 Å and 9710 Å. The shape of the features clearly suggests that the absorption is due to atomic lines, and we identify all six to be due to absorption of Ti I (a5F-z5Fo). The reason why these lines of Ti I can be seen probably is their particularly low ground state energy. The energy levels of the identified lines are taken from *The Atomic Line List v2.04*²; they are given in Table 3.

Table 3. Infrared Ti I lines, transition type E1, term designation is a5F-z5Fo for all lines

Wavelength in Air	J–J	level energies [cm ^{−1}]
9599.55 Å	3-4	6661.00 – 17075.31
9638.26 Å	5-5	6842.96 – 17215.44
9647.37 Å	2-3	6598.75 – 16961.42
9675.50 Å	4-4	6742.76 – 17075.31
9688.80 Å	1-2	6556.83 – 16875.19
9705.68 Å	3-3	6661.00 – 16961.42

5.2. 2MASS 0532+8246

The optical and infrared spectrum of 2MASS 0532+8246 has been investigated by B03. The $1.5 - 2.4 \mu\text{m}$ region is quite unlike any known late-type M, L, or T-dwarf spectrum, which B03 attribute to collision induced H_2 absorption centered near $2.5 \mu\text{m}$, enhanced due to metal-deficiency. The optical and J -band region they show, however, is very similar to that of the L7 dwarf DENIS 0205–1159 AB, and B03 suggest that 2MASS 0532+8246 is a metal-poor late L-dwarf similar to DENIS 0205–1159 AB. The main differences with DENIS 0205–1159 AB are the bands of metal hydrides and TiO, which are stronger in 2MASS 0532+8246 consistent with a metal-poor atmosphere. B03 suggest that the TiO bands are enhanced because production of Ti-bearing condensates is inhibited in the Ti depleted atmosphere, leaving Ti and O for TiO.

The high-resolution spectrum we obtained of 2MASS 0532+8246 is of lower quality than the one shown in the previous Section for LSR 1610–0040. Nevertheless, in the red part of the spectrum, data quality is high enough to compare the Rb I and Cs I lines redward of 8700 \AA to a spectrum of DENIS 0205–1159 AB we took with HIRES at Keck in December 1997. We plot parts of both spectra in the two panels of Fig. 5. The spectrum we have of DENIS 0205–1159 AB only extends to 8700 \AA . The other parts of our high resolution spectrum of 2MASS 0532+8246 are plotted together with the spectrum of the L1 field dwarf 2MASS 1439+1929 in Fig. 6.

5.2.1. Metal oxides

In M-type subdwarfs, absorption bands of metal oxides like TiO and VO are weaker than they are in M-dwarfs of higher metallicity. TiO bands become saturated in mid M-dwarfs then weaken in late M- and L-dwarfs due to condensation of Ti into refractory dust grains. The TiO band at 8430 \AA is stronger in 2MASS 0532+8246 than it is in DENIS 0205–1159 AB, as mentioned by B03. This implies that the formation of dust is more inhibited than the formation of TiO in the metal-poor atmosphere of 2MASS 0532+8246. The TiO band at 8870 \AA is compared to the L1 dwarf 2MASS 1439+1929 in the top panel of Fig. 6. Both have comparably strong TiO bands, i.e., the TiO band of 2MASS 0532+8246 is as strong as is in a metal rich L1 dwarf, and much stronger than in a normal metallicity dwarf of spectral type L7.

²<http://www.pa.uky.edu/~peter/atomic/>

5.2.2. *Metal hydrides*

The FeH and CrH bands at 9900 Å and 9970 Å, respectively, are stronger than in any other late type dwarf known to date (bottom panel of Fig. 6). Their strength can be interpreted as a direct consequence of the enhanced hydride band strength in metal-poor atmospheres.

A detection of TiH at 9400 Å in the spectrum of 2MASS 0532+8246 shown in B03 was claimed by Burgasser et al. (2004b), and Burrows et al. (2005) showed that spectral features of TiH at this wavelengths may not be weak. Strong TiO absorption bands together with strongly enhanced bands of FeH and CrH support the expectation that 2MASS 0532+8246 is a very good candidate for a detection of TiH absorption. We show the region around 9400 Å of our spectrum of 2MASS 0532+8246 compared to the spectrum of 2MASS 1439+1929 and the telluric reference spectrum of HR 153 in the second panel of Fig. 6. We did not adjust the spectra for their radial velocities, in order to show the matching sets of telluric lines due to H₂O. There is no positive evidence of TiH in the 9380–9407 Å region of our high resolution spectrum. All visible absorption features are narrow and clearly not rotationally broadened. They also match the features visible in 2MASS 1439+1929 and the telluric reference. Thus, TiH absorption is not detected in the high-resolution spectrum of 2MASS 0532+8246.

5.2.3. *Atomic lines*

The spectral quality in the blue part of the spectrum of 2MASS 0532+8246 is not very high. We cannot reliably follow the spectrum around the K I line at 7700 Å. The bluest detected spectral feature is the Rb I line at 7950 Å. Another atomic alkali line clearly detected is the Cs I line at 8520 Å. Both regions are shown together with the spectrum of the L7 dwarf DENIS 0205–1159 AB in Fig. 5. The strong alkali lines of DENIS 0205–1159 AB are accurately reproduced by the spectrum of 2MASS 0532+8246, possibly indicating comparable temperatures in both objects.

No lines of Ca II or Ba I are detected in 2MASS 0532+8246. Since these lines are expected to be comparably weak, they can be easily hidden in the noise since they would be broadened by the strong surface rotation. Cs I is also detected at 8940 Å but we have no comparison spectrum of DENIS 0205–1159 AB in that region. Comparison to 2MASS 1439+1929 shows that Cs I is much stronger than it is in the L1 dwarf, as expected.

We show the spectral region around 9640 Å in the third panel of Fig. 6. B03 detected an unidentified absorption feature in that region. We have shown in Sect. 5.1.3 that atomic Ti absorption lines are remarkably strong in that spectral region in LSR 1610–0040. The

major absorption features visible in the spectrum of 2MASS 0532+8246 are located at the same wavelengths, and we conclude that a great part of the unidentified absorption is due to atomic Ti.

The strongest absorption line at 9640 Å appears to have a very strong red wing; this cannot be attributed to the fast rotation velocity which only marginally broadens the line compared to the intrinsic width visible in the spectra of LSR 1610–0040 and 2MASS 1439+1929. We looked at synthetic spectra at this spectral region and found that this red wing also appears in spectra at temperatures around 2000 K. This absorption is probably due to lines of FeH which cover the region from 9590 to 9700 Å. They particularly show a cluster of lines at 9643 Å³, which we identified as a (0–0) band, particularly the ${}^4\Delta_{3/2} - {}^4\Delta_{5/2}$ transition (Phillips et al. 1987). Since FeH is particularly strong in the spectrum of 2MASS 0532+8246, it appears plausible that FeH shows up in this spectral region as well, although it has not yet been observed in other L-dwarfs. A second FeH bandhead, the ${}^4\Delta_{5/2} - {}^4\Delta_{7/2}$ transition, may also be visible at 9600 Å. Both bandheads split into two different parities (a–a) and (b–b). We marked them in the third panel of Fig. 6.

6. Resolving the Alkali Line Conundrum in LSR 1610–0040

We return now to the apparent inconsistencies in the spectrum of LSR 1610–0040, and the question of whether it is really M or L, and metal-poor or not. We first compare the appearance of the Rb I and Cs I lines in LSR 1610–0040 to spectra of Gl 406 (M5.5V) and 2MASS 1439+1929 (L1). We wish to investigate why the Rb I lines of LSR 1610–0040 resemble the lines 2MASS 1439+1929 while the Cs I lines of LSR 1610–0040 resemble those of Gl 406. We compare the spectra of LSR 1610–0040 and 2MASS 1439+1929 to synthetic spectra calculated with the PHOENIX code (Allard et al. 2001, we use the DUSTY models and assume $\log g = 5.5$ for both objects). The temperature scale in Golimowski et al. (2004) produces an estimate of the temperature of $T_{\text{eff}} \approx 2200$ K for 2MASS 1439+1929 (L1), and we use a temperature of 2800 K for comparison to Gl 406. We adopt the hypothesis that this is the temperature appropriate to LSR 1610–0040, and test models with metallicities of $[\text{Fe}/\text{H}] = 0$ and -1 .

In the left panel of Fig. 4 we show the three observed spectra and two models for the Rb I line at 7800 Å. The lines in LSR 1610–0040 and 2MASS 1439+1929 are very similar (LSR 1610–0040 has a slight broader one). Gl 406 has the weakest, narrowest line. The model with solar metallicity most closely resembles Gl 406; although the line depth is deeper

³We thank P.H. Hauschildt for investigating absorption features in PHOENIX model spectra.

the line wings end at almost the same width. The metal-deficient model, on the other hand is as deep as LSR 1610–0040 and 2MASS 1439+1929, and has wings which are broad, but not quite broad enough to match them. The molecular pseudo-continua around the line also match the two cases. We caution that the models still have deficiencies, and the normalization of the spectra is a matter of (consistent) choice, but the general agreements are heartening.

The right panel of Fig. 4 shows a similar analysis for the Cs I line at 8521Å. The spectra are all normalized as in Fig. 2, namely outside the TiO band at 8430Å. The great difference between Gl 406 and 2MASS 1439+1929 in Cs I is quite obvious, although the similar strengths of the background TiO leaves their pseudo-continua at similar levels. The solar metallicity model has a similar level, and the line is sharper and deeper than Gl 406, but nothing like the strength of the line for the L dwarf. Lowering the metallicity yields a line strength and pseudo-continuum level that is a better match to LSR 1610–0040. We thus obtain a reasonable fit to both the Rb I *and* Cs I lines of LSR 1610–0040 using approximately $T_{\text{eff}} = 2800$ K, $[\text{Fe}/\text{H}] = -1$. This is why we would assign it a spectral type of sd?M6. The reason for the disparate line strengths in Gl 406 compared with LSR 1610–0040 is the weakened background opacity in LSR 1610–0040, which allows the line wings of Rb I (but not Cs I, which is less abundant) to be revealed, while they remain hidden by TiO in Gl 406. This is also the reason for the increased strengths of the Ba I and Ca II lines in LSR 1610–0040 compared to Gl 406.

7. Conclusions

We have presented the first high resolution spectra of the peculiar possibly metal-poor sd?M6 LSR 1610–0040 and the late-type L-subdwarf 2MASS 0532+8246. We have derived accurate radial and rotation velocities for both objects, and we compared their spectral features to spectra of known field L-dwarfs. The spectra of LSR 1610–0040 and 2MASS 0532+8246 are very different in many respects. These are discussed below.

The radial velocity of LSR 1610–0040 is consistent with the value reported by L03 if we assume that their determination suffered similar systematic effects as mentioned by B03 for the case of 2MASS 0532+8246. For the latter, we derive a radial velocity consistent with the result of B03. We computed the space motion in order to check membership of the halo population. Our result for LSR 1610–0040 significantly differs from the result reported by L03; the radial velocity of LSR 1610–0040 does not fall outside the 2σ -region reported for thick disk stars by Chiba & Beers (2000). However, the V -velocity of LSR 1610–0040 (-111 km s^{-1}) is comparably high, and the space motion vector does not contradict its halo

membership. For 2MASS 0532+8246, our estimate of the V -velocity is $V = -285 \text{ km s}^{-1}$, which is in strong support of halo membership.

The rotation velocity of LSR 1610–0040 is below the detection limit of about 5 km s^{-1} . This is consistent with the bulk of its properties more closely resembling the M5.5V dwarf Gl 406 than an L1 object. We have analyzed the reasons why it was initially classified as an early-L subdwarf, and explain them with a mild metal-deficiency. For the true L subdwarf, 2MASS 0532+8246, we measure a rotation velocity of $v \sin i = 65 \text{ km s}^{-1}$. If this object is indeed a relic of the young galaxy, that means that the braking time for a mid L-dwarf is much longer than 10 Gyr. Either the braking time exceeds the age of the galaxy by this spectral type, or there is no rotational braking in mid to late L-type objects at all.

In M-subdwarfs metal-oxides are weaker and metal-hydrides are stronger than in the metal rich M-dwarfs, but both species are stronger in 2MASS 0532+8246 than in its metal-rich counterpart DENIS 0205–1159 AB. The strong oxide-bands in 2MASS 0532+8246 can be explained by invoking a reduced level of dust formation in the metal-deficient atmosphere, which would leave behind more TiO than in the metal rich L-dwarfs (B03). The extremely strong metal-hydride bands in 2MASS 0532+8246 are generally consistent with observations of enhanced metal-hydride bands in M-subdwarfs.

Chemistry and line formation in the ultracool atmospheres of L-dwarfs is much more complex than it is in hotter stars because of dust formation and depletion of refractory metals from the atmosphere. The chemical anomalies of subdwarfs heighten these complexities, and currently yield a confusing situation. High-resolution spectra provide crucial information for our eventual understanding of the ultracool metal-deficient atmospheres which were common in the early galaxy.

Based on observations obtained from the W.M. Keck Observatory, which is operated as a scientific partnership among the California Institute of Technology, the University of California and the National Aeronautics and Space Administration. We would like to acknowledge the great cultural significance of Mauna Kea for native Hawaiians and express our gratitude for permission to observe from atop this mountain. We thank P.H. Hauschildt for providing high-resolution versions of spectra calculated with PHOENIX, and for an identification run on some of them. GB thanks the NSF for grant support through AST00-98468. AR has received research funding from the European Commission’s Sixth Framework Programme as an Outgoing International Fellow (MOIF-CT-2004-002544).

REFERENCES

- Ackerman, A.S., & Marley, M.S. 2001, ApJ, 556, 872
- Allard, F., Hauschildt, P.H., Alexander, D.R., Tamanai, A., & Schweitzer, A., 2001, ApJ, 556, 357
- Andersson, N., Balfour, W.J., Bernath, P.F., Lindgren, B., & Ram, R.S., 2003, JChPh., 118, 3543
- Bailer-Jones, C.A.L., 2004, A&A, 419, 703
- Basri, G., Mohanty, S., Allard, F., Hauschildt, P.H., Delfosse, X., Martín, E.L., Forveille, T., & Goldman, B., 2000, ApJ, 538, 337
- Burgasser, A.J., Marley, M.S., Ackerman, A. S., et al., 2002, ApJ, 571, 151
- Burgasser, A.J., 2004a, ApJ, 614, L76
- Burgasser, A.J., et al., 2003, ApJ, 592, 1186, (B03)
- Burgasser, A., Kirkpatrick, J. D., & Lépine, S. 2004, in Cool Stars, Stellar Systems, and the Sun 13 (ESA SP; Noordwijk: ESA), in press
- Burrows, A., Dulick, M., Bauschlicher, C.W. Jr., Bernath, P.F., Ram, R.S., Sharp, C.M., & Milsom, J.A., 2005, ApJ, 624, 988
- Cushing, M.C., & Vacca, W.D., 2005, [arXiv:astro-ph/0511398](#)
- Delfosse, X., Forveille, T., Perrier, C., & Mayor, M., 1998, A&A, 331, 581
- Chiba, M., & Beers, T.C., 2000, AJ, 119, 2843
- Gizis, J.E., 1997, AJ, 113, 806
- Golimowski, D.A., Leggett, S.K., Marley, M.S., et al., 2004, AJ, 127, 3516
- Kirkpatrick, J.D., Reid, I. N., Liebert, J., et al., 1999, ApJ, 519, 802
- Kuiper, G.P., 1939, ApJ, 89, 548
- Liebert, J., Kirkpatrick, J.D., Cruz, K.L., Reid, I.N., Burgasser, A., Tinney, C.G., Gizis, J.E., AJ, 125, 343
- Lépine, S., Rich, R.M., M.M., S., 2003a, AJ, 125, 1598,

- Lépine, S., Rich, R.M., M.M., S., 2003b, ApJ, 591, L49, (L03)
- Lodders, K., 2002, ApJ, 577, 974
- Martín, E.L., Basri, G., Delfosse, X., & Forveille, T., 1997, A&A, 327, L29
- Monet, D.G., et al., 1992, AJ, 103, 806
- Mohanty, S., Basri, G., Shu, F., Allard, F., Chabrier, G. 2002, ApJ, 571, 469
- Mohanty, S., & Basri, G., 2003, ApJ, 583, 451
- Mohanty, S., Basri, G., Jayawardhana, R., Allard, F., Hauschildt, P., & Ardila, D., 2004, ApJ, 609, 854
- Mould, J.R., 1976, ApJ, 207, 535
- Noll, K.S., Geballe, T.R., Marley, M.S. 1997, ApJ, 489, L87
- Oppenheimer, B.R., Kulkarni, S.R., Matthews, K., & van Kerkwijk, M.H. 1998, ApJ, 502, 932
- Phillips, J.G., Davis, S.P., Lindgren, B., & Balfour, W.J., 1987, ApJ, 65, 721
- Scholz, R.-D., Lehmann, I., Matute, I., & Zinnecker, H., 2004a, A&A, 425, 519
- Scholz, R.-D., Lodieu, N., & McCaughrean, M.J., 2004b, A&A, 428, L25
- Westphal, J.A., Matthews, K., & Terrile, R.J. 1974, ApJ, 188, L111

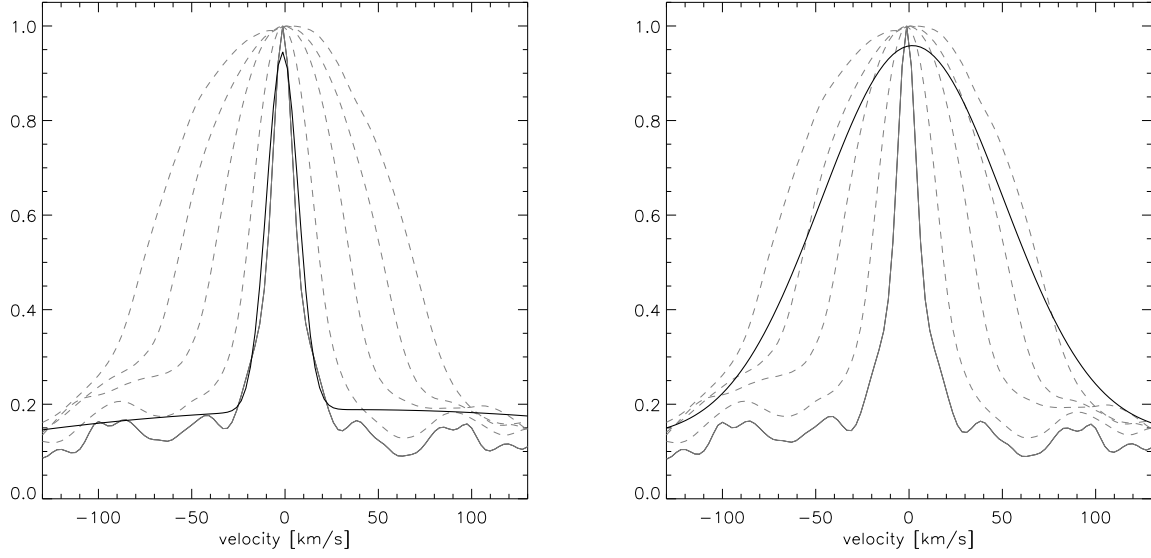


Fig. 1.— Cross correlation function of Gl406 and LSR 1610–0040 (left panel) and 2MASS0532+8246 (right panel). Correlation functions of the spectrum of Gl406 with a version of that template spun up by $v \sin i = 0, 20, 40, 60, 80 \text{ km s}^{-1}$, in order of the narrowest to widest curves, are overplotted for calibration (dashed lines).

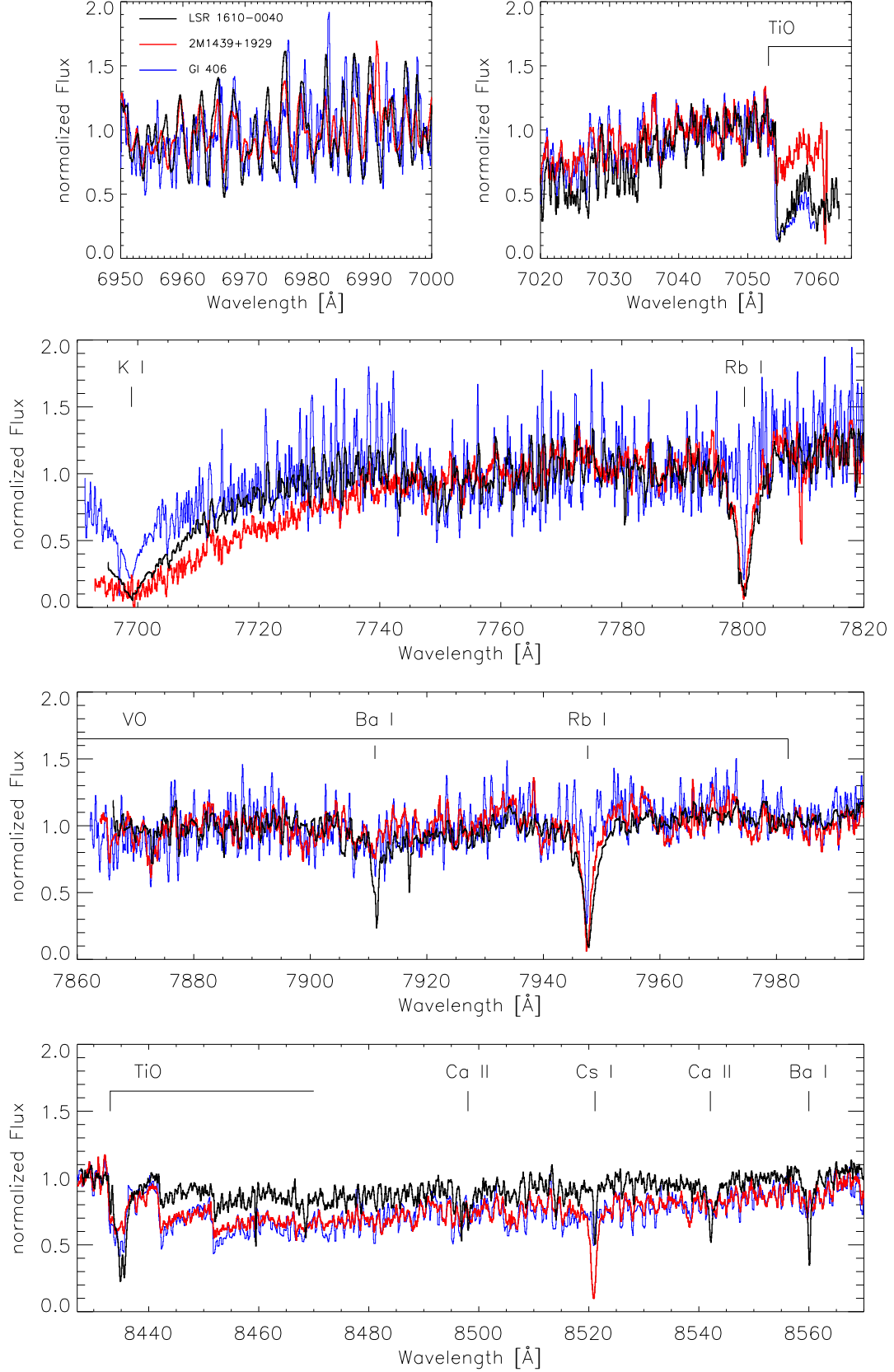


Fig. 2.— Spectra of LSR 1610–0040 (black), the L1 field L-dwarf 2MASS 1439+1929 (red) and the M5.5 dwarf Gl 406 (blue). The two narrow features in the TiO bandhead at 8435 Å

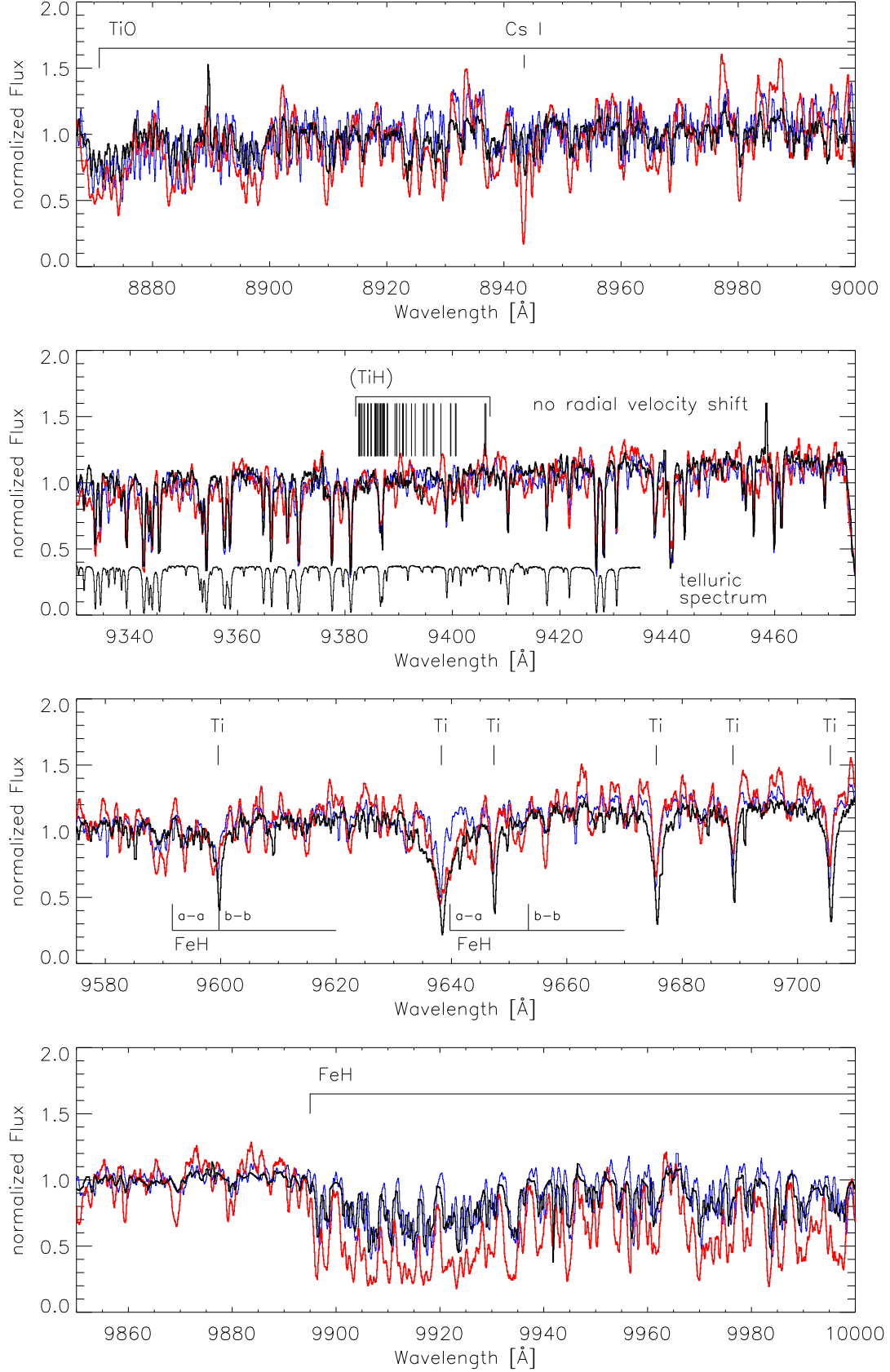


Fig. 3.— Spectra of LSR 1610–0040 (black), the L1 field L-dwarf 2MASS 1439+1929 (red) and the M5.5 dwarf Gl 406 (blue).

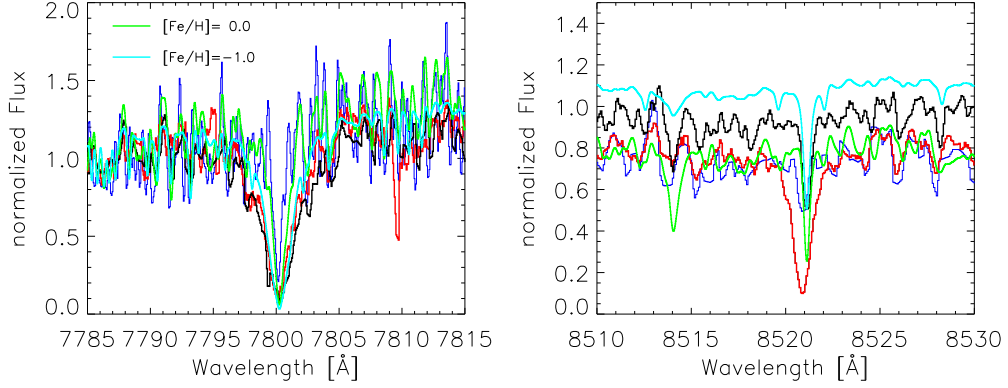


Fig. 4.— Rb and Cs lines as shown in Fig. 2. Two models at $T_{\text{eff}} = 2800$ K are overplotted; solar metallicity $[\text{Fe}/\text{H}] = 0.0$ (green) and metal deficient $[\text{Fe}/\text{H}] = -1.0$ (cyan).

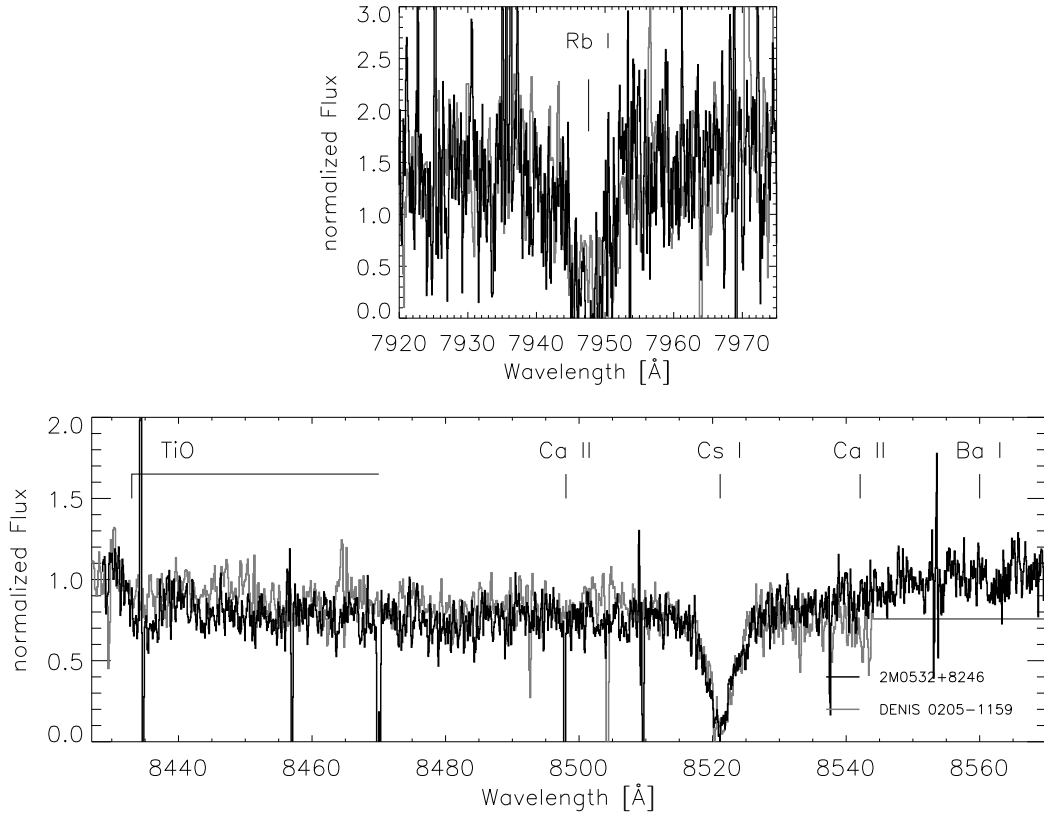


Fig. 5.— Spectra of the late-type L-subdwarf 2MASS 0532+8246 (black line) compared to the L7 field dwarf DENIS 0205-1159 AB (grey line).

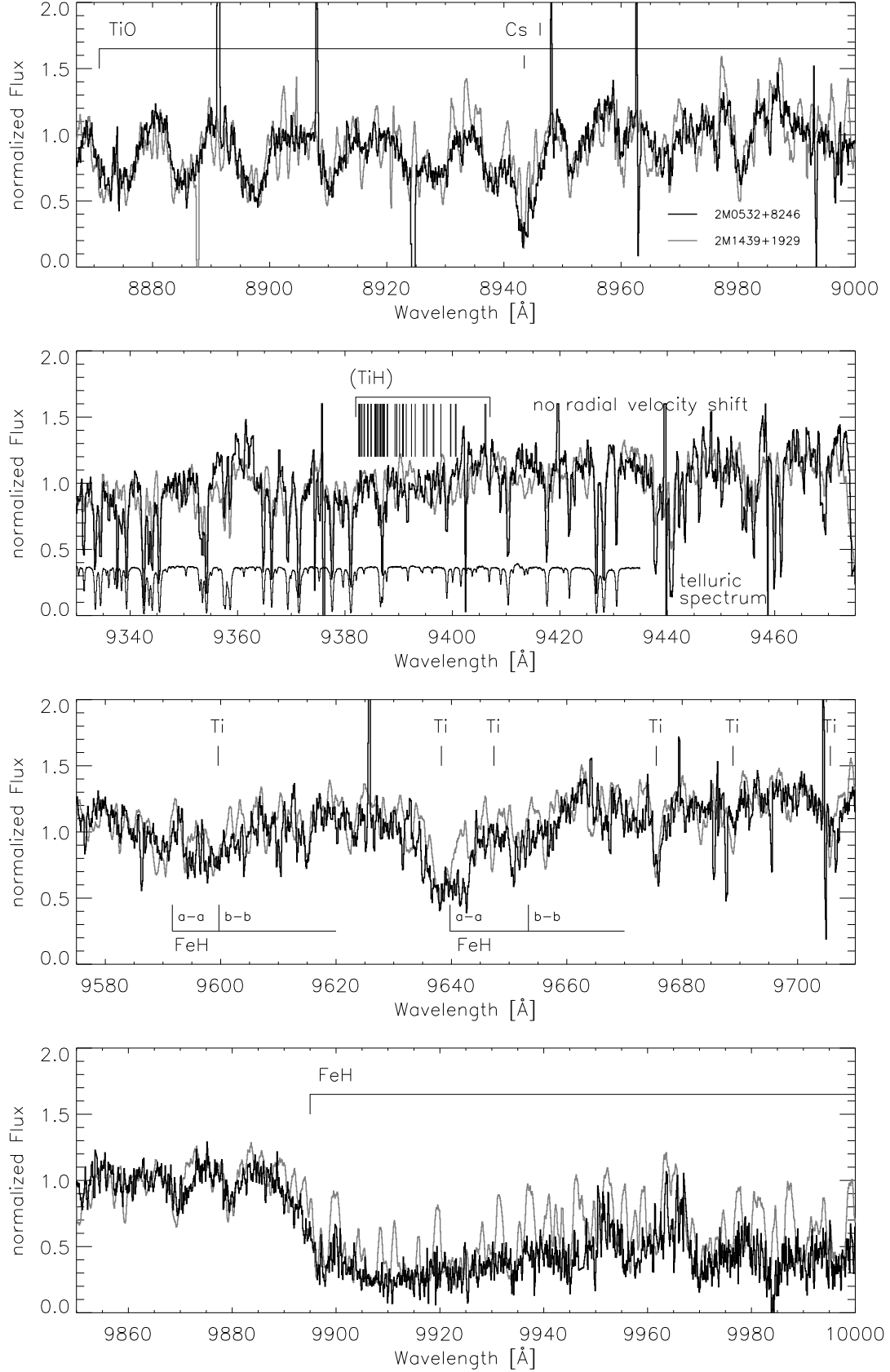


Fig. 6.— Spectra of the late-type L-subdwarf 2MASS 0532+8246 (black line) compared to the L1 field dwarf 2MASS 1439+1929 (grey line). Our spectrum of DENIS 0205–1159 AB